In Situ Synthesis of C/Cu/ZnO Porous Hybrids as Anode Materials for Lithium Ion Batteries

Yuyan Wang,[†] Xiaojian Jiang,[†] Lishan Yang,[‡,§,*] Ning Jia,[†] and Yi Ding[†]

[†]Center for Advanced Energy Materials & Technology Research (AEMT), School of Chemistry and Chemical Engineering, Shandong University, Jinan, 250100, China

[‡]Key Laboratory of Chemical Biology & Traditional Chinese Medicine Research, Ministry of Education, College of Chemistry and Chemical Engineering, Hunan Normal University, Changsha, Hunan 410081, China

[§]School of Materials Science and Engineering, Shandong University, Jinan, 250061 China

ABSTRACT: Porous structure and surface modification have been widely studied in applying metal oxide nanomaterials as Li-ion battery anodes for overcoming problems such as poor conductivity and large volume variation. Here, we demonstrate a direct triple-decomposition process for the in situ synthesis of C/Cu/ZnO porous hybrids. In a typical porous structure, 5−10 nm sized ZnO and Cu nanoparticles aggregate randomly and are modified with carbon layers in thickness of 1 nm. Moreover, the resulted hybrid nanostructures show a high and stable specific capacity of 818 mAh g^{-1} at a current rate of 50 mA g^{-1} with almost 100% capacity retention for up to 100 cycles when used an anode material for lithium ion batteries.

By combination of the structural analyses and electrochemical behaviors, it could be speculated that the porous structure and the modifications of copper nanoparticles and carbon layers are mainly responsible for the dramatically improved electrochemical performance of ZnO anodes.

KEYWORDS: in situ synthesis, porous, hybrid, carbon layer, lithium ion battery
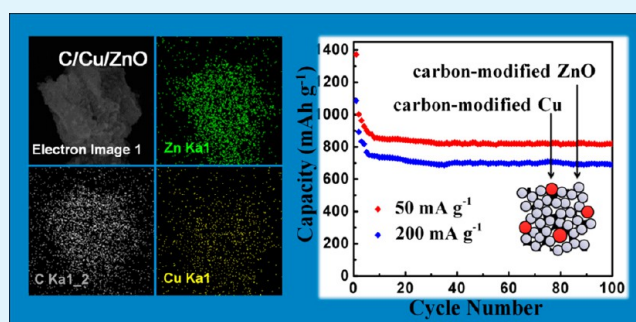
1. INTRODUCTION

Considering that rechargeable Li-ion batteries (LIBs) almost dominate the portable electronic and electric vehicle markets, it is highly desired to further improve the battery performance by developing new electrode materials with higher specific capacity, better conductivity, and better cycle stability.[1−3] Significant achievements have been gained in the pertinent research of anode materials with superior capacity,[4] in which metal oxides (M_xO_y, M = Co, Fe, Cu, Sn, Zn, etc.) have received special attention because of their low-cost, easy availability, and much higher theoretical capacities in contrast to the commercial graphite counterpart.[5−10] However, various disadvantages such as poor conductivity and large volume variation have to be overcome before the practical application of M_xO_y materials. At present, admirable strategies to improve the performance of M_xO_y electrodes would involve (i) preparing nano-sized M_xO_y materials (e.g. sheets, rods, wires, spheres, flowers, polyhedrons, and so on) to reduce the Li$^+$ diffusion lengths;[11−15] (ii) surface-modifying M_xO_y with conductive materials (e.g. carbon nanotubes, graphene, Cu nanorods, Ni foam, conductive polymers, and so on) for better conductivities;[16−21] and (iii) applying porous structures to alleviate the volume changes of M_xO_y crystals.[22−25] Actually, it is difficult to pack nano-sized powder as densely on the current collector as micrometer-sized materials, which will result in a low tap density of the electrodes and a decrease in the final cell capacity.[2] A more practical way to apply M_xO_y nanomaterials into electrodes would be to use micrometer-sized hybrids that consist of assembled and modified M_xO_y nanoparticles.

Among various potential M_xO_y materials, zinc oxide (ZnO) is proven to be a promising anode candidate for their multiple Li storage behaviors via the alloying/dealloying reactions, and thus, large theoretical capacities are expected (978 mAh g^{-1}).[14] To really get a high and reversible capacity, ZnO anodes always possess both high electronic conductivity and stable porosity nanostructure. For example, a hybrid micro-structure with uniform distribution of ZnO nanoparticles into the porous carbon host could render superior cyclability to pure ZnO nanoparticles, which was ascribed to the strong binding of ZnO to carbon and the morphological stability endowed by their micropores during battery cycles.[26] Interestingly, porous ZnO nanosheets grown on Cu substrates also exhibited much better conductivity and higher capacity than the ZnO nanopowder, even if only the ZnO nanosheet edge contacted with the Cu substrate.[27] Regarding the modification over ZnO conductivity, carbon can be designed to be various porous or coating structures with excellent adhesion. On the other hand, metal Cu also seems to be a better alternative due to the higher

electronic conductivity (5.96×10^7 S m^{-1}) than carbon (2×10^5 to 3×10^5 S m^{-1}) and amorphous carbon (1.25×10^3 to 2×10^3 S m^{-1}).[28−30] On the basis of the above analyses, an ideal ZnO model might be an integration of these three features: ZnO micromaterial with a porous structure to alleviate the volume changes and shorten the Li$^+$ diffusion length; the modification of copper nanomaterials to increase the electrical conductivity of ZnO; and the carbon coatings to inhibit ZnO from structural changes during cycling and direct contact with the electrolyte solution.[31]

Keeping such considerations in mind, we designed a novel triple-decomposition process for the synthesis of C/Cu/ZnO porous nanohybrids, where ZnO and Cu nanoparticles were well modified with C, and this triple-decomposition process was designed based on different decomposition behaviors of ZnC$_2$O$_4$, CuC$_2$O$_4$ and polyvinylpyrrolidone (PVP).[32−34] As shown in Figure 1, PVP-coated oxalate particles are firstly

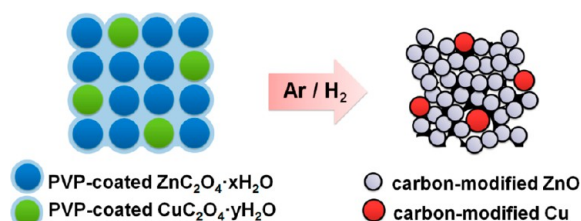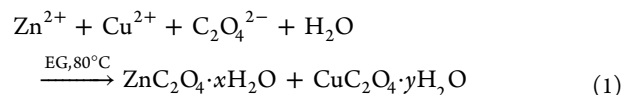**Figure 1.** Schematic depiction of the transformation from mixed Cu^{2+}/Zn^{2+} oxalates particles into C/Cu/ZnO hybrid porous nanostructures.

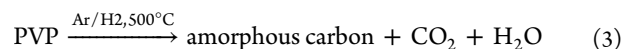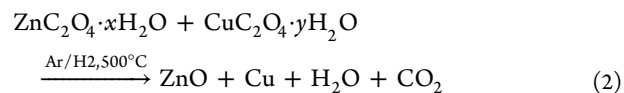formed by the co-deposition reaction of Zn^{2+} as well as Cu^{2+} between C$_2$O$_4^{2-}$ in PVP glycol solution (step 1). Under calcination, the oxalates particles will release CO$_2$ and H$_2$O to generate C/Cu/ZnO porous hybrids (step 2). The reaction equations can be expressed as follows.

Step 1:

$$Zn^{2+} + Cu^{2+} + C_2O_4^{2-} + H_2O$$

$$\xrightarrow{\text{EG,80°C}} ZnC_2O_4 \cdot xH_2O + CuC_2O_4 \cdot yH_2O \qquad (1)$$

Step 2:

$$ZnC_2O_4 \cdot xH_2O + CuC_2O_4 \cdot yH_2O$$

$$\xrightarrow{\text{Ar/H2,500°C}} ZnO + Cu + H_2O + CO_2 \qquad (2)$$

$$PVP \xrightarrow{\text{Ar/H2,500°C}} \text{amorphous carbon} + CO_2 + H_2O \qquad (3)$$

In our study, the C/Cu/ZnO porous hybrids afford reversible capacities of 818 mAh g^{-1} at 50 mA g^{-1}, and 689 mAh g^{-1} at 200 mA g^{-1} after 100 cycles, much better than C/ZnO and pure ZnO porous nanostructures.

2. EXPERIMENTAL SECTION

Synthesis of Mixed Cu^{2+}/Zn^{2+} Oxalate Precursors. In a typical synthesis, 0.01 mol Cu(ac)$_2$·H$_2$O, 0.04 mol Zn(ac)$_2$·2H$_2$O and 5 g PVP were dissolved in 240 mL ethylene glycol (EG) in a 500 mL flask, and heated in an oil bath at 80 °C for 20 min under magnetic stirring. Then, 60 mL EG solution containing 0.83 mol/L oxalic acid dihydrate was added to the Cu^{2+}/Zn^{2+} solution at a rate of 3.75 mL/min. The mixed solution was stirred and kept in the oil bath at 80 °C for 4 h. The products were collected by centrifugation, washed twice with ethanol, and finally dried under vacuum at 150 °C for 4 h.

Synthesis of C/Cu/ZnO Porous Hybrids. The C/Cu/ZnO porous hybrids were synthesized by annealing the as-prepared oxalate precursors at 500 °C for 2 h in an Ar/H$_2$ atmosphere, with an
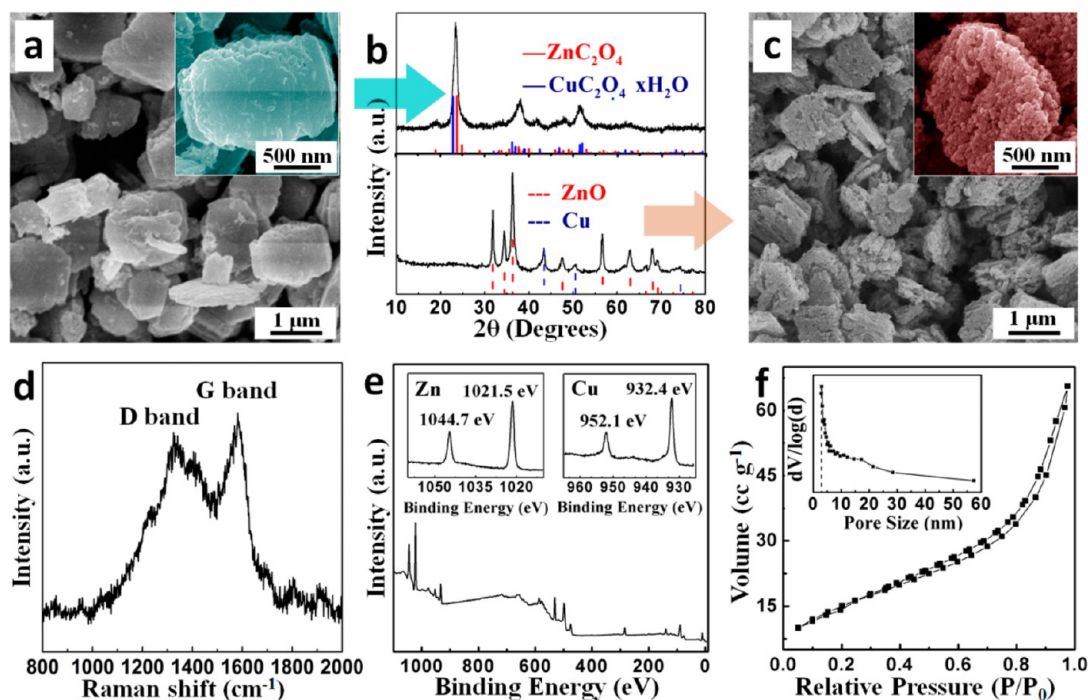

Figure 2. SEM images of the oxalate precursors (a) and the C/Cu/ZnO hybrid products (c). (b) XRD patterns of the oxalate precursor (ZnC$_2$O$_4$ (JCPDS#37-0718), CuC$_2$O$_4$·xH$_2$O (JCPDS#21-0297)) and the hybrid product (ZnO (JCPDS#36-1451), Cu (JCPDS#04-0836)). (d) Raman spectra of the C/Cu/ZnO hybrid products. (e) XPS survey spectra of C/Cu/ZnO hybrid products; inset is the spectra of Zn (left) and Cu (right). (f) The N$_2$ adsorption/desorption isotherm of the C/Cu/ZnO hybrids; inset is the corresponding pore size distribution curve. Both the precursors and products are synthesized with a Cu:Zn molar ratio of 1:4.

increasing rate of 5 °C/min. Similarly, C/Cu/ZnO hybrids with different Cu:Zn molar ratio could be obtained by varying the Cu^{2+}/Zn^{2+} molar ratio within a constant total amount ($Cu^{2+} + Zn^{2+} = 0.05$ mol) in the preparation of oxalate precursors, and the pure ZnO nanomaterials were formed by annealing the C/ZnO hybrids at 600 °C for 2 h in air.

Characterizations. The XRD patterns were obtained by using a Bruker D8 advanced X-ray diffractometer with Cu Kα radiation (λ = 1.54178 Å). The morphologies of the final products were characterized by SEM (Hitachi X650) and HRTEM (JEOL JEM-2100). Elemental analysis was performed on XPS (ESCALAB 250) and EDS (EDAX Genesis 4000). The N_2 adsorption/desorption isotherms were obtained by a Quadrasorb SI analyzer at 77 K. The Raman spectrum was recorded at ambient temperature on a LABRAM-HR confocal laser MicroRaman spectrometer. The mass fractions of carbon were calculated from the elemental analysis tests by a Elementar Vario Max CN Analyzer.

Electrochemical Test. The electrochemical cells were assembled as CR2032-type coin cells composed of a C/Cu/ZnO electrode, a Li metal counter electrode, a polymer membrane separator (Celgard 2300), and an organic electrolyte of 1 mol/L $LiPF_6$ in a 1:1 mixture of ethylene carbonate and dimethyl carbonate. The working electrode was prepared by coating the slurry of C/Cu/ZnO, Super-P carbon black, and carboxymethylcellulose sodium (CMC) (7:2:1 in weight ratio) onto a Cu foil, and then dried at 80 °C for 12 h. CV profiles were obtained in the range of 0.1−3.0 V at a scanning rate of 0.1 mV s^{-1} with an electrochemical workstation (CHI 760C, Shanghai, China). Galvanostatic discharge−charge cycling was performed between 0.1 V and 3.0 V on a lithium battery cycler (LAND CT-2001A, Wuhan, China) at room temperature. Electrochemical impedance spectroscopy (EIS) was carried out on an electrochemical workstation (Materials Mates 520, Italia) connected to a Potentiostat-510 (Materials Mates) in the frequency range from 0.1 MHz to 0.01 Hz. All the electrode capacities were calculated by using the ZnO content as the only active material in the each hybrid.

3. RESULTS AND DISCUSSION

The mixed Cu^{2+}/Zn^{2+} oxalate particles with a diameter of ∼1 μm were firstly synthesized via a PVP-assisted oxalate co-precipitation process with a Cu:Zn molar ratio of 1:4 (Figure 2a). Followed by direct thermal annealing at 500 °C under an Ar/H_2 atmosphere, the PVP-coated Cu^{2+}/Zn^{2+} mixed oxalate particles were converted into the C/Cu/ZnO porous hybrids with a similar shape (Figure 2c). It was reported that ZnC_2O_4, CuC_2O_4 and PVP could produce ZnO, metal Cu and amorphous carbon via corresponding decompositions below 400 °C in inert atmosphere.[32] In the present synthesis, H_2 can avoid the oxidation of Cu by the trace amounts of oxygen in the tube furnace, and high annealing temperature (500 °C) favors the decomposition of precursors and the crystallization of products. Powder X-ray diffraction (XRD) patterns in Figure 2b prove the composition transformation from mixed Cu^{2+}/Zn^{2+} oxalates (ZnC_2O_4 (JCPDS#37-0718), $CuC_2O_4\cdot xH_2O$ (JCPDS#21-0297)) into related hybrids composed of ZnO (JCPDS#36-1451) and Cu (JCPDS#04-0836). The Raman spectrum (Figure 2d) shows a D-band at 1329 cm^{-1} and a G-band at 1582 cm^{-1} with similar intensities, confirming an amorphous carbon structure in the C/Cu/ZnO hybrid.[35] X-ray photoelectron spectroscopy (XPS) was employed to further investigate the chemical composition and chemical state of the synthesized C/Cu/ZnO porous hybrids (Figure 2e). Peaks located at 1021.5 and 1044.7 eV can be attributed to Zn 2p$_{3/2}$ and Zn 2p$_{1/2}$ for ZnO. Moreover, in the Cu spectrum, Cu2p$_{3/2}$, Cu2p$_{1/2}$ binding energies which appear at about 932.4 and 952.1 eV can be regarded as a precise identification of Cu^0, further confirming that $CuC_2O_4\cdot xH_2O$ has been transformed

into metal Cu completely. The porous structure characteristics and Brunauer−Emmett−Teller (BET) specific surface area of the C/Cu/ZnO hybrid with a Cu:Zn molar ratio of 1:4 were investigated by nitrogen isothermal adsorption (Figure 2f), showing a BET specific surface of ∼56.1 m^2 g^{-1} and a pore distribution centered ∼3.0 nm.

In a typical porous hybrid structure, numerous 5−15 nm sized ZnO and Cu nanocrystals are stacked together randomly to obtain a porous structure (Figure 3a). The selected area
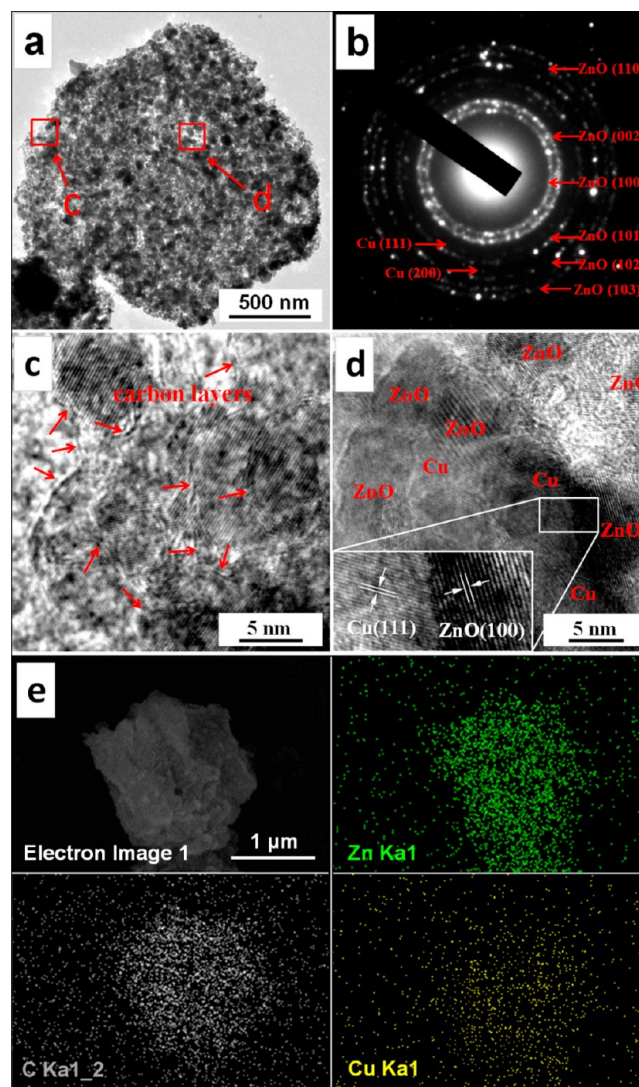

Figure 3. (a) TEM image of a typical C/Cu/ZnO porous hybrid nanostructure. (b) The corresponding SAED pattern. (c, d) HRTEM images taken from the edge and the internal parts of the hybrid nanostructure in part a. (e) Element maps of C/Cu/ZnO show the segregated distribution of Zn (green), Cu (yellow), and C (gray) in a hybrid particle. All the hybrids have a Cu:Zn molar ratio of 1:4.

electron diffraction (SAED) pattern is shown in Figure 3b, wherein the ring-like diffraction mode demonstrates the polycrystalline nature of ZnO/Cu constituents of the porous hybrids. Those ZnO and Cu nanoparticles are modified with amorphous carbon layers of 1 nm thick (Figure 3c). As shown in the HRTEM image of Figure 3d, ZnO nanoparticles with a ∼5 nm size disperse with the Cu nanoparticles (5−10 nm) in the random way. Insert image in Figure 3d further reveals a locally magnified HRTEM result taken from a heterojunction

structure of two adjacent nanoparticles. The marked interplanar d-spacings correspond to the (111) lattice planes of cubic Cu and the (100) lattice planes of hexagonal ZnO. A uniform distribution of zinc, copper, and carbon can be seen and demonstrated by the EDS elemental mappings (Figure 3e).

We studied the hybrids with other Cu:Zn molar ratios, the phase purity and chemical composition of hybrids were detected by EDS analysis (Figure 4). The corresponding
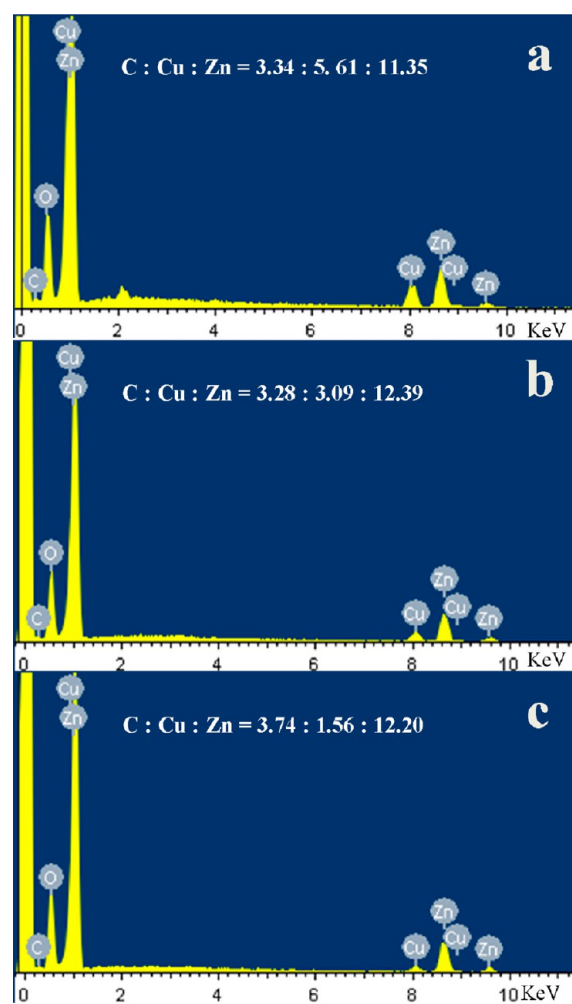
Table 1. Surface Area Data and Elemental Analysis of the Synthesized Samples

material[a]	BET surface area ($m^2 g^{-1}$)	pore diam. (nm)	pore vol. (cm^3/g)	content of carbon (wt %)
C/Cu/ZnO (1:8)	48.386	3.043	0.083	3.45
C/Cu/ZnO (1:4)	56.123	3.052	0.090	3.41
C/Cu/ZnO (1:2)	33.209	4.387	0.070	3.65
C/ZnO	46.911	3.092	0.081	3.37
ZnO	38.257	4.157	0.074	0.45

[a]Here, C/Cu/ZnO (Cu:Zn = 1:x) is marked as C/Cu/ZnO (1:x).

in Figure 5a confirm the component changes of ZnO (JCPDS#36-1451) and Cu (JCPDS#04-0836) in these samples. Furthermore, the relative intensity of Cu peak increased with the increasing content of Cu. The cycling performance of pure ZnO, C/ZnO, and C/Cu/ZnO porous hybrids were recorded at 200 mA g^{-1} (Figure 5b). It is found that C/ZnO has a similar first discharge capacity with pure ZnO while the former obtains a more stable cyclability due to the carbon coatings. By comparison, C/Cu/ZnO electrodes exhibit much higher discharge capacities than C/ZnO and pure ZnO electrodes. As the Cu:Zn molar ratio was adjusted from 1:8 to 1:4, and 1:2, the first discharge capacities of the C/Cu/ZnO hybrid increased from 1003 to 1086, and 1104 mAh g^{-1}. In all, C/Cu/ZnO (1:4) holds the best cycling stability (689 mAh g^{-1} at 200 mA g^{-1} after 100 cycles.) among the five samples, which may result from high BET surface area, high electrical conductivity and structure stability.

The increased electric conductivities of the C/Cu/ZnO hybrids with the composites of Cu and C were supported by electrochemical impedance spectra (EIS) testing. Figure 5c shows the Nyquist plots of the corresponding ZnO electrodes operated at room temperature after ten discharge−charge cycles in the fully charged state, in which all EIS spectra are similar and composed of a semicircle in the high-to-medium frequency region and a slope line in the low frequency region. The numerical value of the diameter of the semicircle on the Z_{re} axis gives an approximate indication of the charge transfer resistance (R_{ct}), and the straight line with a slope of approximately 45° in a low frequency region corresponds to the Li$^+$ diffusion process within electrodes.[36−38] It is apparent that the R_{ct} values of C/Cu/ZnO hybrids are much lower than those of the C/ZnO and pure ZnO, which can be attributed to the faster charge transfer by incorporating of Cu and C to porous ZnO materials. The reduction of the charge transfer resistance can furnish the C/Cu/ZnO hybrids with enhanced electron and Li$^+$ transportation during the electrochemical reactions, and hence, improve the Li$^+$ storage performance of the C/Cu/ZnO hybrids. Besides, all the five semicircles in Figure 5c are a bit depressed, which is probably due to the mesoporous structure of the electrode materials as reports.[39] Considering that the Cu:Zn (1:4) hybrid possessed the best cycling stability (689 mAh g^{-1} at 200 mA g^{-1} after 100 cycles) along with the highest surface area (56.123 $m^2 g^{-1}$) and pore volume (0.090 cm^3/g), we thought the 1:4 molar ratio was an optimum choice in this study.

Additionally, cyclic voltammetry (CV) was used to test the pure ZnO, C/ZnO, and C/Cu/ZnO (1:4) anodes for the first 3 cycles at a scan rate of 0.1 mV s^{-1} (Figure 6). According to previous reports, the board reduction peak around 0.25 V in the

Figure 4. EDS spectrum from the synthesized C/Cu/ZnO hybrids with different Cu and ZnO molar ratios: (a) Cu:Zn ≈ 1:2, (b) Cu:Zn ≈ 1:4, (c) Cu:Zn ≈ 1:8.

results display that C/Cu/ZnO (1:4) possesses the highest surface area among the pure ZnO or ZnO-based hybrids (Table 1). Compared to pure ZnO, the amorphous carbon coating can help the porous ZnO to obtain a higher surface area (46.911 m^2 g^{-1} vs 38.257 $m^2 g^{-1}$). And the C/Cu/ZnO (1:4) possesses the largest pore volume (0.090 cm^3/g). Also, we find low carbon contents in the composites (Figure 4), which are consistent with the carbon elemental analytic results (Table 1), that is, about 3.37 wt % C content in C/ZnO, and 3.65, 3.41, 3,45 in C/Cu/ZnO (1:2), C/Cu/ZnO (1:4), and C/Cu/ZnO (1:8).

To shed light on the influences of metal copper and carbon on C/Cu/ZnO hybrids, we evaluated the electrochemical and structural properties of pure ZnO, C/ZnO, and C/Cu/ZnO (Cu:Zn = 1:2, 1:4, 1:8) by XRD, galvanostatic cycling and electrochemical impedance spectra. The XRD patterns shown

1528

dx.doi.org/10.1021/am404181q | ACS Appl. Mater. Interfaces 2014, 6, 1525−1532
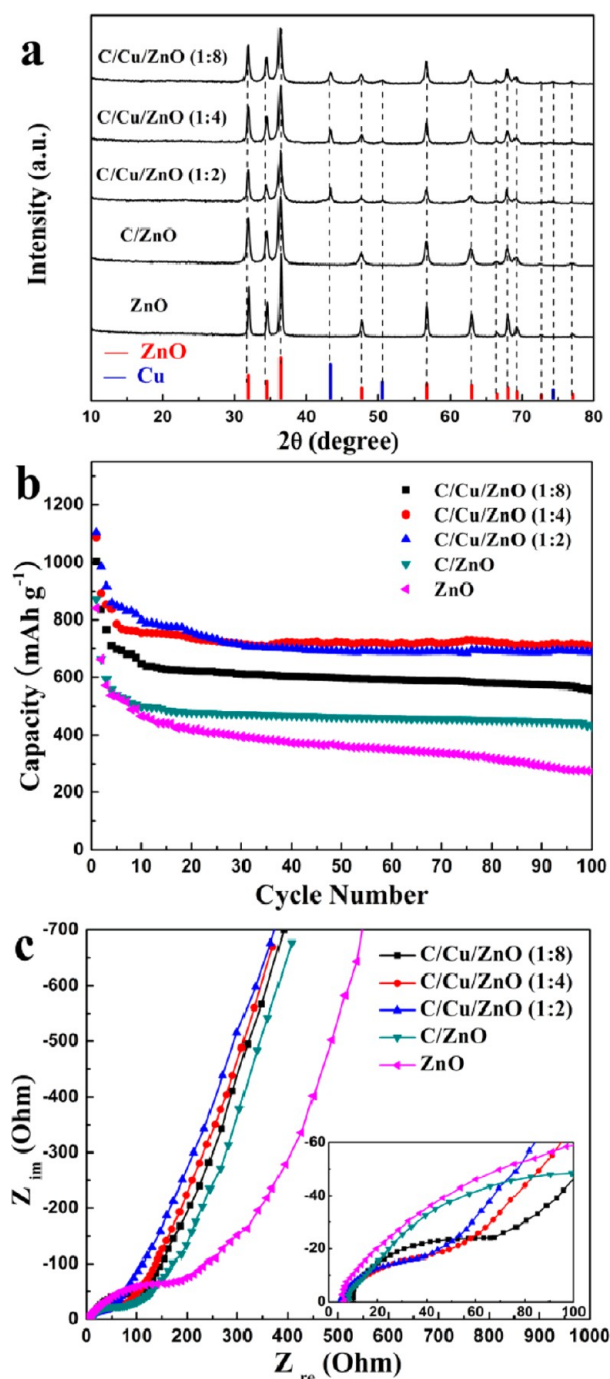
Figure 5. (a) XRD patterns of pure ZnO, C/ZnO, and C/Cu/ZnO porous hybrids with different Cu:Zn molar ratios; (b) the corresponding cycling performance at 200 mA g^{-1}; (c) the corresponding Nyquist impedance plots after 10 cycles, insets show the high frequency part of the plots. Here, C/Cu/ZnO (Cu:Zn = 1:x) is marked as C/Cu/ZnO (1:x).

Figure 6. CV curves of (a) pure ZnO, (b) C/ZnO hybrid, (c) C/Cu/ZnO (1:4) hybrid, at 0.1 mV s^{-1}.

first scan of pure ZnO electrode (Figure 6a) could be responses to the multiple reduction processes from ZnO into Zn^{0}, the generations of Li−Zn alloy and the SEI layer.[14,26] In the subsequent second and third cycles, the cathodic peak shifts to the potential range 0.5−1.0 V, which corresponds to the reduction of ZnO and the formation of amorphous Li$_2$O.[14] During the subsequent anodic scan there are several oxidation peaks in the potential range 0.25−0.8 V, which correspond to a multistep dealloying process of Li−Zn alloy (LiZn, Li$_2$Zn,
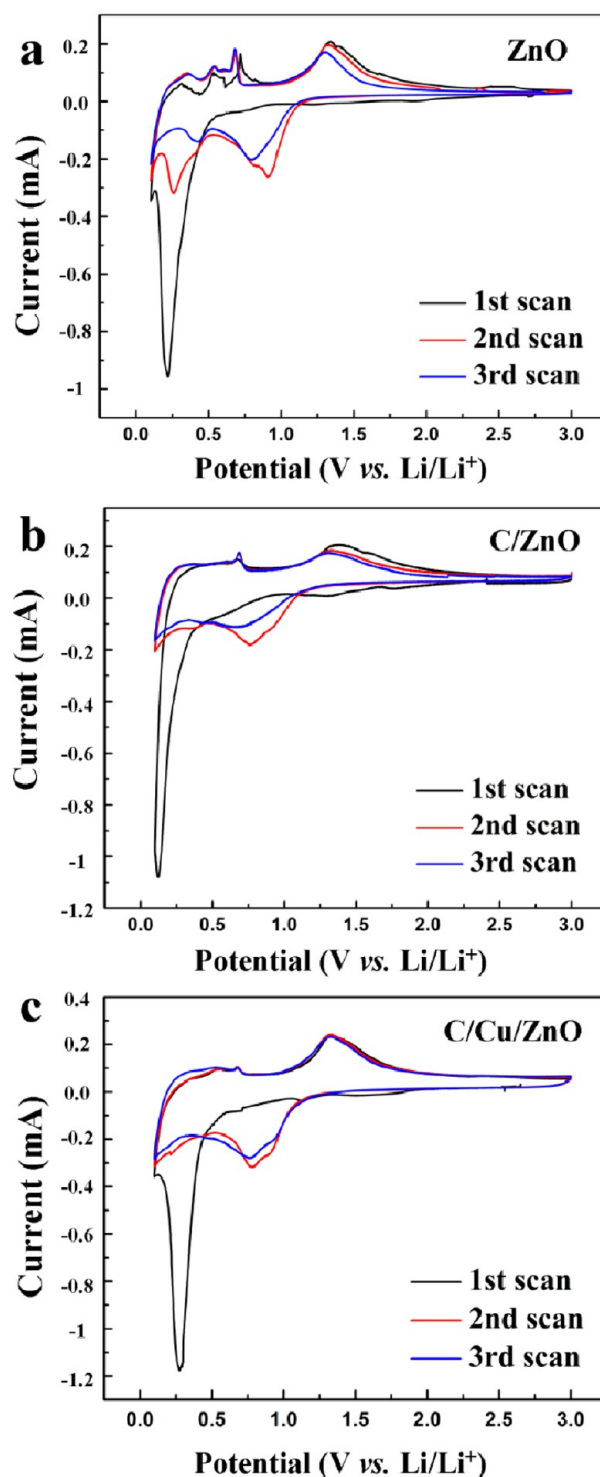
LiZn$_2$, and Li$_2$Zn$_5$) and the decomposition of SEI layer.[14] In addition, a strong and broad oxidation peak around 1.4 V may be indicated as the decomposition of Li$_2$O.[27] In contrast, the multistep dealloying reduction peaks (at 0.25−0.8 V) of C/ZnO and C/Cu/ZnO hybrids overlap to form a broad peak (Figure 6b and c). Similar results have been reported and concluded as conductive additives (such as carbon coatings and Cu nanoparticles in this study) could serve as catalysts to alleviate the dealloying process of Li−Zn alloys and the
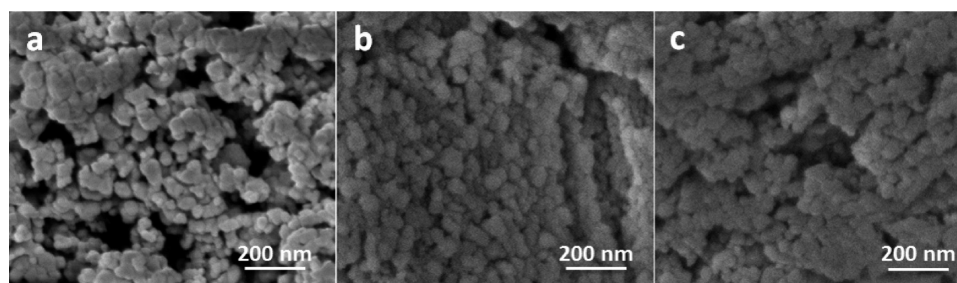
Figure 7. TEM images of C/Cu/ZnO (1:4) porous hybrids selected: (a) before battery cycling, (b) 10 cycles, and (c) 100 cycles at a current rate of 200 mA g^{-1}.
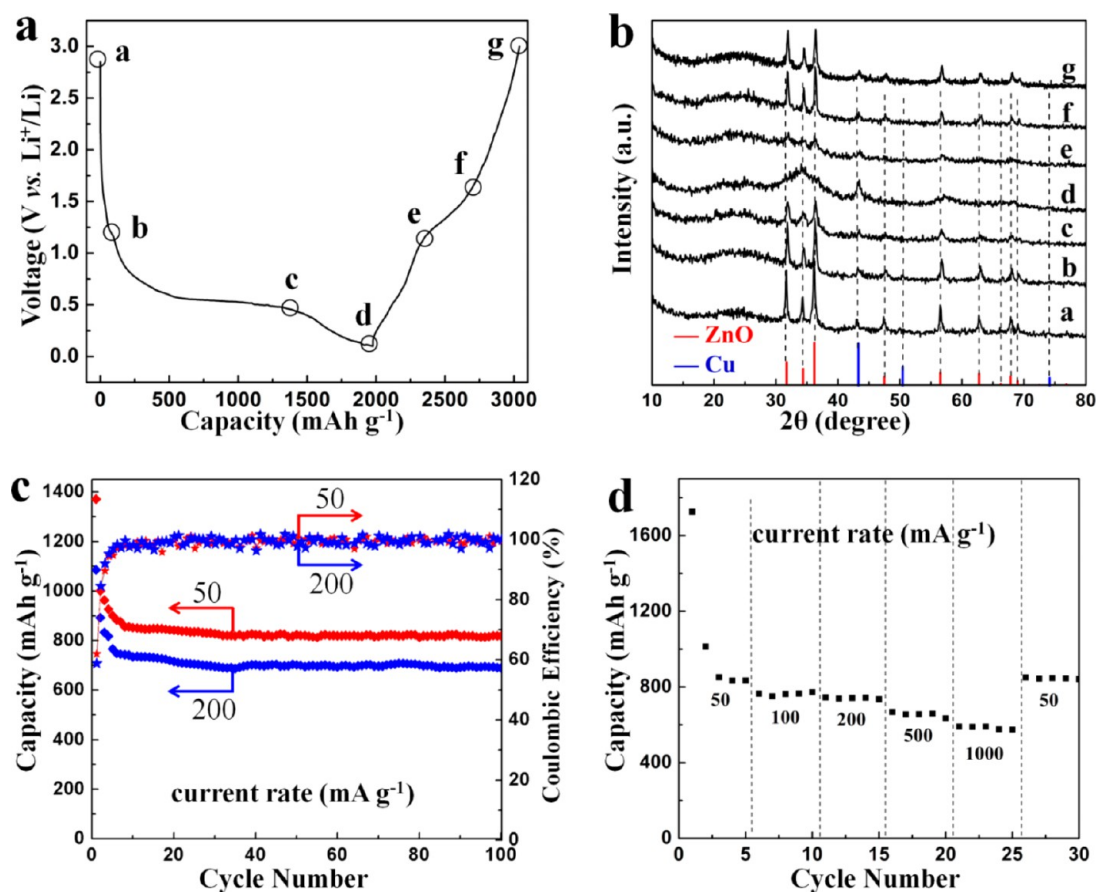

Figure 8. (a) Discharge/charge profiles of C/Cu/ZnO (1:4) electrode for the first cycle at a current rate of 30 mA g^{-1}; a–g denote the states of different lithiated materials for the corresponding ex situ X-ray patterns were taken. (b) Ex situ XRD patterns collected at various states of the cells. (c) Cycling performance and coulombic efficiencies of the C/Cu/ZnO (1:4) hybrids at 50 and 200 mA g^{-1}. (d) Rate capabilities of the C/Cu/ZnO (1:4) hybrids at different current rates.

decomposition of Li$_2$O, which could finally improve the reversible capability of the ZnO electrods.[14,42,44] Compared to the pure ZnO and C/ZnO electrodes, the CV curves of the C/Cu/ZnO electrode at second and third cycles are more stable; its peak current and the integrated peak area of the C/Cu/ZnO are much higher, indicating the C/Cu/ZnO electrode has higher capacity and reversibility than the pure ZnO and C/ZnO electrodes.

C/Cu/ZnO (1:4) hybrids were employed as the anode active materials in LIBs. SEM images of C/Cu/ZnO (1:4) hybrids selected before and after battery cycles show that the surface of those nanoparticles became rough and the pores within grew unobvious after battery operations (Figure 7). To further study the changes of electrode materials during the cycling, a series of

partially lithiated cells are measured at different depth of discharge (DOD, %) during the first galvanostatic discharge/charge. The samples at a–g points in Figure 8a were collected for the ex situ XRD measurement (see Figure 8b). During the first discharge process from 2.8 V to 0.1 V, the plateau starting from 0.75 V represents the reduction of ZnO, the alloying reaction between Li and Zn^0, and the growth of solid electrolyte interphase (SEI) layer.[22] At the beginning of the charge process (d–e in Figure 8a), the multistep delithiation reaction of Li$_x$Zn happens below 1.0 V. The XRD patterns (e–g in Figure 8b) show the emergence and growth of ZnO as more and more lithium is extracted. The galvanostatic charge/discharge results agree well with the reduction/oxidation peaks in the CV analysis of the C/Cu/ZnO hybrid. Usually, oxide-based anodes

Table 2. Comparisons of Cycling Performance among Different ZnO Anodes

electrode material	1st cycle discharge/charge capacity (mAh g^{-1})	capacity/cycle (mAh g^{-1})	potential range (V)	current density (mA g^{-1})	ref.
ZnO nanorods	1461/980	310/40th	0.0–3.0	0.1 mA cm^{-2}	40
Porous ZnO nanosheets	1120/750	400/100th	0.01–3.0	50	41
ZnO microrod arrays	790/620	500/100th	0.02–3.0	500	42
ZnO nanotubes	932/621	386/50th	0.01–2.5	0.5 C	43
Ni/ZnO	1048/786	490/30th	0.02–3.0	80	44
Au/ZnO flowers	1280/660	392/50th	0.02–3.0	120	14
Se/ZnO	703/–	422/50th	0.01–3.5	0.005 mA cm^{-2}	45
CNT/ZnO	1610/968	602/50th	0.0–3.0	100	46
ZnO-M/PC	2107.4/1062.9	653.7/100th	0.1–3.0	100	26
C/Cu/ZnO (1:4)	1372/962.1	818.7/100th	0.1–3.0	50	this work
C/Cu/ZnO (1:4)	1086.2/873.8	689.9/100th	0.1–3.0	200	this work

are classified into three groups depending on the reaction mechanisms: (i) Li-alloy reaction, (ii) intercalation reaction, and (iii) conversion reaction.[1,5] Based on the above results, the conversion reaction mechanism of Li$^+$ with the ZnO electrode in this study can be expressed as follows:

$$ZnO + 2Li^+ + 2e^- \leftrightarrow Zn^0 + Li_2O \qquad (4)$$

$$Zn^0 + xLi^+ + xe^- \leftrightarrow Li_xZn \qquad (5)$$
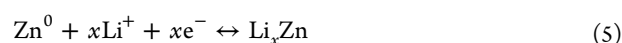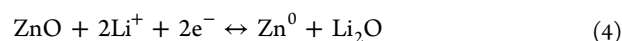
As an anode material, ZnO has a theoretical capacity of 978 mAh g^{-1} and the ZnO-based battery performance could be obviously affected by its structures and the conductive loadings.[5,14] In this work, the cycling performance of the C/Cu/ZnO hybrid is depicted between 0.1 V and 3.0 V (Figure 8c). The first discharge/charge capacities are 1372–962 mAh g^{-1} at 50 mA g^{-1}, and 1086–873 mAh g^{-1} at 200 mA g^{-1}. Both the first discharge capacities are higher than the theoretical capacity of ZnO, which can be attributed to the formation of a SEI layer and possible interfacial lithium storage.[2,22] After 100 cycles, the discharge capacities of the C/Cu/ZnO hybrids at 50 and 200 mA g^{-1} are 818 mAh g^{-1} and 689 mAh g^{-1}, respectively. To the best of our knowledge, this is the best result among the recent reports (Table 2). Also, its coulombic efficiency after the 5th cycle maintains at about 100%. Furthermore, the C/Cu/ZnO electrode also indicates excellent rate performance (Figure 8d). As the current densities increase from 50 to 100, 200, 500, 1000 mA g^{-1}, the electrode exhibits good capacity retention, varying from 838 to 756, 732, 650, 565 mAh g^{-1}, respectively. Remarkably, after the high rate measurement, when the current density returns to 50 mA g^{-1}, the discharge capacity of about 831 mAh g^{-1} can be recovered.

4. CONCLUSIONS

C/Cu/ZnO porous hybrids were obtained through an in situ triple decomposition process. The as-synthesized C/Cu/ZnO hybrids are composed of numerous carbon-modified ZnO and Cu nanoparticles. As anode materials, the C/Cu/ZnO porous hybrids exhibit reversible capacities of 818 mAh g^{-1} at 50 mA g^{-1}, and 689 mAh g^{-1} at 200 mA g^{-1} after 100 cycles. The enhanced electrochemical performances are ascribed to the modifications of Cu and C, along with the porous structures. Furthermore, this multiple decomposition reaction method can be designed for the general in situ synthesis of various metal/oxide, or oxide/oxide, or carbon-modified hybrid nanomaterials.

■ AUTHOR INFORMATION

Corresponding Author

*Tel: +86 531 88366513. Fax: +86 531 88366269. E-mail: lsyang.chemistry@gmail.com.

Notes

The authors declare no competing financial interest.

■ REFERENCES

(1) Bruce, P. G.; Scrosati, B.; Tarascon, J. M. Angew. Chem., Int. Ed. 2008, 47, 2930–2946.
(2) Goodenough, J. B.; Kim, Y. Chem. Mater. 2010, 22, 587–603.
(3) Jiang, J.; Li, Y. Y.; Liu, J. P.; Huang, X. T.; Yuan, C. Z.; Lou, X. W. Adv. Mater. 2012, 24, 5266–5180.
(4) Goodenough, J. B. Acc. Chem. Res. 2013, 46, 1053–1061.
(5) Reddy, M. V.; Subba Rao, G. V.; Chowdari, B. V. R. Chem. Rev. 2013, 113, 5364–5457.
(6) Poizot, P.; Laruelle, S.; Grugeon, S.; Dupont, L.; Tarascon, J. M. Nature 2000, 407, 496–499.
(7) Wu, C. Z.; Yin, P.; Zhu, X.; Ouyang, C. Z.; Xie, Y. J. Phys. Chem. B 2006, 110, 17806–17812.
(8) Chen, J. S.; Tan, Y. L.; Li, C. M.; Cheah, Y. L.; Luan, D. Y.; Madhavi, S.; Boey, F. Y. C.; Archer, T. A.; Lou, X. W. J. Am. Chem. Soc. 2010, 132, 6124–6130.
(9) Zhou, X. S.; Wan, L. J.; Guo, Y. G. Adv. Mater. 2013, 25, 2152–2157.
(10) Chen, L.; Xu, H. Y.; Li, L. E.; Wu, F. F.; Yang, J.; Qian, Y. T. J. Power Sources 2014, 245, 429–435.
(11) Wu, P.; Du, N.; Zhang, H.; Zhai, C. X.; Yang, D. R. ACS Appl. Mater. Interfaces 2011, 3, 1946–1952.
(12) Xie, Y.; Wu, C. Z. Dalton Trans. 2007, 45, 5235–5240.
(13) Malik, R.; Burch, D.; Bazant, M.; Ceder, G. Nano Lett. 2010, 10, 4123–4127.
(14) Ahmad, M.; Shi, Y. Y.; Nisar, A.; Sun, H. Y.; Shen, W. C.; Wei, M.; Zhu, J. J. Mater. Chem. 2011, 21, 7723–7729.
(15) Wang, B.; Chen, J. S.; Wu, H. B.; Wang, Z. Y.; Lou, X. W. J. Am. Chem. Soc. 2011, 133, 17146–17148.
(16) Leroux, F.; Koene, B. E.; Nazar, F. J. J. Electrochem. Soc. 1996, 143, 181–183.
(17) Taberna, P. L.; Mitra, S.; Poizot, P.; Simon, P.; Tarascon, J. M. Nat. Mater. 2006, 5, 567–573.

1531

dx.doi.org/10.1021/am404181q | ACS Appl. Mater. Interfaces 2014, 6, 1525–1532

(18) Nam, K. T.; Kim, D. W.; Yoo, P. J.; Chiang, C. Y.; Meethong, N.; Hammon, P. T.; Chiang, Y. M.; Belcher, A. M. *Science* **2006**, *312*, 885−888.

(19) Wang, L.; Xu, H. W.; Chen, P. C.; Zhang, D. W.; Ding, C. X.; Chen, C. H. *J. Power Sources* **2009**, *193*, 846−850.

(20) Liu, D. Q.; Yang, Z. B.; Wang, P.; Li, F.; Wang, D. S.; He, D. Y. *Nanoscale* **2013**, *5*, 1917−1921.

(21) Nam, S. H.; Shim, H. S.; Kim, Y. S.; Dar, M. A.; Kim, J. G.; Kim, W. B. *ACS Appl. Mater. Interfaces* **2010**, *2*, 2046−2052.

(22) Jiao, F.; Bruce, P. G. *Adv. Mater.* **2007**, *19*, 657−660.

(23) Wang, H. L.; Cui, L. F.; Yang, Y.; Casalongue, H. S.; Robinson, J. T.; Liang, Y. Y.; Cui, Y.; Dai, H. J. *J. Am. Chem. Soc.* **2010**, *132*, 13978−13980.

(24) Liu, H.; Wang, G. X.; Liu, J.; Qiao, S. Z.; Ahn, H. *J. Mater. Chem.* **2011**, *21*, 3046−3052.

(25) Huang, H.; Zhu, W. J.; Tao, X. Y.; Xia, Y.; Yu, Z. Y.; Fang, J. W.; Gan, Y. P.; Zhang, W. K. *ACS Appl. Mater. Interfaces* **2012**, *4*, 5974−5980.

(26) Shen, X. Y.; Mu, D. B.; Chen, S.; Wu, B. R.; Wu, F. *ACS Appl. Mater. Interfaces* **2013**, *5*, 3118−3125.

(27) Huang, X. H.; Xia, X. H.; Yuan, Y. F.; Zhou, F. *Electrochim. Acta.* **2011**, *56*, 4960−4965.

(28) Giancoli, D.C. In *Physics for Scientists and Engineers with Modern Physics*, 4th ed.; Jocelyn, P. Prentice Hall: Upper Saddle River, New Jersey, 2009; p 658.

(29) Pauleau, Y.; Péter, B. B.; Barna, P. B. In *Protective Coatings and Thin Films: Synthesis, Characterization, and Applications*; Kluwer Academic/Springer: New York, 1997; p 215.

(30) Pierson, H. O. In *Handbook of Carbon, Graphite, Diamond, and Fullerenes: Properties, Processing, and Applications*; Noyes Publications: Park Ridge, NJ, 1993; p 61.

(31) Lee, K.T.; Jeong, S.; Cho, J. *Acc. Chem. Res.* **2013**, *46*, 1161−1170.

(32) Dollimore, D. *Thermochim. Acta* **1987**, *117*, 331−363.

(33) Donkova, B.; Mehandjiev, D. *J. Mater. Sci.* **2005**, *40*, 3881−3886.

(34) Du, Y. K.; Yang, P.; Mou, Z. G.; Hua, N. P.; Jiang, L. *J. Appl. Polym. Sci.* **2006**, *99*, 23−26.

(35) Tuinstra, F.; Koenig, J. L. *J. Chem. Phys.* **1970**, *53*, 1126−1130.

(36) Wei, X. Q.; Man, B. Y.; Liu, M.; Xue, C. S.; Zhuang, H. Z.; Yang, C. *Phys. B* **2007**, *388*, 145−152.

(37) Espinós, J. P.; Morales, J.; Barranco, A.; Caballero, A.; Holgado, J. P.; González-Elipe, A. R. *J. Phys. Chem. B* **2002**, *106*, 6921−6929.

(38) Zhong, C.; Wang, J. Z.; Chou, S. L.; Konstantinov, K.; Rahman, M.; Liu, H. K. *J. Appl. Electrochem.* **2010**, *40*, 1415−1419.

(39) Shi, Z. C.; Attia, A.; Ye, W. L.; Wang, Q.; Li, Y. X.; Yang, Y. *Electrochim. Acta* **2008**, *53*, 2665−2673.

(40) Wang, H. B.; Pan, Q. M.; Cheng, Y. X.; Zhao, J. W.; Yin, G. P. *Electrochim. Acta* **2009**, *54*, 2851−2855.

(41) Pan, Q. M.; Qin, L. M.; Liu, J.; Wang, H. B. *Electrochim. Acta* **2010**, *55*, 5780−5785.

(42) Huang, X. H.; Wu, J. B.; Lin, Y. R.; Guo, Q. *Int. J. Electrochem. Sci.* **2012**, *7*, 6611−6621.

(43) Park, K. T.; Xia, F.; Kim, S. W.; Kim, S. B.; Song, T.; Paik, U.; Park, W. I. *J. Phys. Chem. C* **2013**, *117*, 1037−1043.

(44) Zhang, C. Q.; Tu, J. P.; Yuan, Y. F.; Huang, X. H.; Chen, X. T.; Mao, F. *J. Electrochem. Soc.* **2007**, *154*, A65−A69.

(45) Zhou, Y. N.; Li, W. J.; Fu, Z. W. *Electrochim. Acta* **2012**, *59*, 435−440.

(46) Abbas, S. M.; Hussain, S. T.; Ali, S.; Ahmad, N.; Ali, N.; Abbas, S. *J. Mater. Sci.* **2013**, *48*, 5429−5436.